IEEE Access
Multidisciplinary ⋮ Rapid Review ⋮ Open Access Journal

Received 10 June 2026, accepted 9 July 2026, date of publication 14 July 2026, date of current version 21 July 2026.

Digital Object Identifier 10.1109/ACCESS.2026.3713404

RESEARCH ARTICLE

Contactless HR Monitoring and HRV Assessment by Attention-Based Fusion Using a Continuous Wave Radar System

HUI LU[1], (Member, IEEE), ROBERT HOLZSCHUH[2], ROBERT FREUND[2], STEFFEN ORTMANN[2,3], DIRK GROSSE MEININGHAUS[2], AND ALEXANDER KOELPIN[1], (Fellow, IEEE)

[1]Hamburg University of Technology, Institute of High-Frequency Technology, 21073 Hamburg, Germany
[2]Medical University Lausitz–Carl Thiem, 03048 Cottbus, Germany
[3]Department of Operative Hospital Management, München Klinik gGmbH, 81925 Munich, Germany

Corresponding author: Hui Lu (hui.lu@tuhh.de)

This work was supported by the Federal Ministry of Education and Research of Germany (BMBF) within the iCampμs 2 Project under Grant 16ME0420k.

This work involved human subjects or animals in its research. Approval of all ethical and experimental procedures and protocols was granted by the ethics committee of Landesärztekammer Brandenburg under Application No. 2023-40-MPDG-ff.

ABSTRACT Continuous wave (CW) radar is an alternative to gold-standard electrocardiography (ECG) for contactless heart rate (HR) monitoring and heart rate variability (HRV) analysis. This work aims to monitor HR and HRV using a deep learning (DL) model with a 61 GHz CW radar system. We employed attention-based DL fusion model to combine information from radar heart sound (HS) and radar pulse wave (PW) signals. Additionally, we compared attention-based fusion with alternative fusion methods, including data fusion, feature fusion, and decision fusion. To evaluate the performance of the proposed method, a dataset of approximately 20 hours was collected from 20 participants in varying body positions. Using attention-based fusion, we achieved the overall highest F1 score of 97.53% for heartbeat detection, which outperformed solely HS-based or PW-based model, as well as other fusion methods. F1 scores exceeding 96% were obtained for all analyzed body positions. A high correlation of 97.11% and an RMSE of 28.99 ms were achieved for the estimation of the interbeat interval (IBI). In addition, we extracted HRV in time, frequency, and nonlinear domains. Low relative errors were achieved, e.g. 14.04% for TRI, 6.14% for LF, 6.35% for alpha2, and 10.93% for ApEn. The proposed approach achieved high-level performance for HR monitoring and HRV estimation using a CW radar system, showing great potential for various healthcare applications.

INDEX TERMS Attention, CW radar, deep learning, fusion, heart rate, heart rate variability, heart sound, pulse wave.

I. INTRODUCTION

Heart rate variability (HRV) describes the variation in intervals between consecutive regular heartbeats [1]. HRV is influenced by heart-brain interactions and regulated by the autonomic nerve system (ANS) [2]. Therefore, HRV provides information about ANS activity and is widely used as an important indicator for various applications, e.g. cardiovascular disease diagnosis [3], stress level [4], sleep monitoring [5], and epileptic seizure monitoring [6]. Electrocardiography (ECG) is the gold-standard for assessing heart rate (HR) and HRV. However, ECG requires continuous contact with the skin, and thus, has downsides of limited mobility and discomfort. Radar system has been studied as an alternative for cardio-respiratory monitoring in a contactless manner [7], [8], [9], [10], [11], [12], [13], [14], [15], [16], [17], [18], [19], [20], [21], [22], [23], [24]. Previous studies have focused on the average HR in a predefined window, making the detection of each heartbeat impossible [7], [8], [9], [10], [11], [12]. However, the accurate timing of each heartbeat is mandatory for assessing HRV.

HRV extraction by continuous wave (CW) radar systems has been investigated in various studies [13], [15], [22], [25], [26], [27], [28]. Hu et al. [13] used the ensemble

The associate editor coordinating the review of this manuscript and approving it for publication was Cheng Hu.

empirical mode decomposition (EEMD) to reconstruct the heart signal and zero-crossing to extract the interbeat interval (IBI). Similarly, Petrovic et al. [15] applied a zero-crossing method after filtering with a set of bands in the frequency range of [0.5, 2.5] Hz. Yen et al. [25] used a filter with a higher frequency band [0.5, 3] Hz to assess heartbeat signals and used peak detection on the derivative heart signal to extract each beat. Sameera et al. [28] filtered the displacement signal from 0.85 Hz to 5 Hz and applied a multi-resolution analysis maximal overlap discrete wavelet transform (MAMODWT) to reconstruct the signal. Template matching was used with peak detection to extract IBI. Edanami et al. [26] proposed a combination of template matching and adaptive peak detection with a filtered signal ranging from 0.75 Hz to 1.5 Hz to extract IBI. However, assuming the radar heart signal to be sinusoidal-like could introduce additional time delays in detecting each beat. In addition, radar systems can measure more complex interactions on the body surface induced by heart action, which contain higher frequency components. Will et al. [16] found various pulse wave (PW) shapes depending on the measured locations on the body by filtering the displacement signal at frequencies up to 15 Hz. A template matching algorithm was implemented to detect instantaneous heartbeats using PW templates [17]. In addition to PW, the heart sound (HS) component of a higher frequency could also be detected by a CW radar system by filtering the radar signals in the frequency range of [16, 80] Hz [18], which is consistent with the expected frequency of heart sound [29]. The onset of the first radar-detected HS coincided closely with the R peak of the ECG signal [18]. A hidden-semi Markov model (HSMM) was implemented to segment heart sound signals and outperformed PW-based template matching [18]. Xie et al. [27] implemented the decoding peak algorithm (DPD) to estimate HRV parameters using radar HS signals, achieving similar performance compared to HSMM. Although the HS-based HRV estimation appears more accurate, it can suffer from lower signal quality due to the relatively small amplitude of HS compared to PW. Low-quality HS signals were observed in different body positions [19]. Therefore, the fusion of PW and HS is necessary to enable an accurate HRV measurement by combining the precision of HS and the strong signal response of PW [20].

With the rapid development of deep learning (DL), significant progress has been made in DL-based extraction of cardiorespiratory parameters using radar systems. Shi et al. [24] applied a DL model using long short-term memory (LSTM) to segment the radar HS signal and extract the HRV parameters. In a previous study [20], fusion of PW and HS was proposed for heartbeat detection using a bidirectional gated recurrent unit (bi-GRU), which is a type of recurrent neural network (RNN) with a simplified structure compared to LSTM. The features extracted with DL models from the PW and HS were fused and the fusion model outperformed the model based solely on the HS. However, only the feature fusion method was considered without taking into account alternative additional fusion approaches. In this paper, we propose three different fusion methods: data fusion, decision fusion, and attention-based fusion. In attention-based fusion, inspired by the successful application of attention modules [30] in language models, we employ self-attention and cross-attention modules to fuse and align the predictions of PW and HS, where these modules compute relationships between elements in the signal sequences to capture contextual dependencies.

To compare the performance of the fusion methods, we collected data from 20 healthy subjects with a total duration of approximately 20 hours of recording in various body positions. Although previous studies that extracted HRV parameters from radar systems focused primarily on the time and frequency domains, HRV in the nonlinear domain has been shown to be relevant in clinical applications, e.g., emotion monitoring [5] and seizure detection [6]. To the best of our knowledge, this study is the first to extract HRV parameters in the nonlinear domain from CW radar signals, demonstrating the feasibility of HRV monitoring in all three domains.

II. METHODS AND MATERIALS

A. RADAR SYSTEM

The CW radar system is shown in Fig. 1. It consists of three stacked mounting building blocks: the radar frontend board, the baseband board, and the interface board. The radar frontend board contains a 30.5 GHz voltage-controlled oscillator (VCO) chip, 61 GHz transceiver (TRX) monolithic microwave integrated circuits (MMIC), a DC-coupled receiver network, and a 4×8 series-fed patch antenna array. The baseband signal from the radar frontend board is digitized by a baseband board and transferred to the STM32 microcontroller evaluation interface board. The digitized radar signals with the synchronization output are transmitted to a computer, enabling synchronization between the radar and the reference system. Further details can be found in [31].

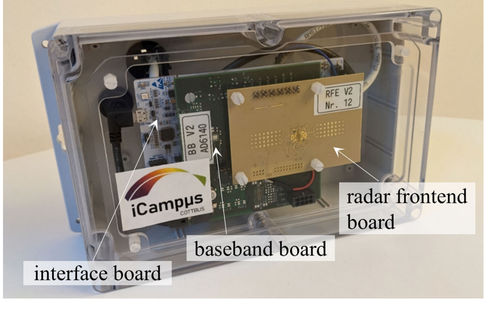

FIGURE 1. Photograph of the CW radar system in housing, reproduced from [31].

The baseband in-phase (I) and quadrature (Q) signals can be described as,

$$I(t) = A_I \cos\left(\frac{4\pi x(t)}{\lambda} + \theta_0\right) + DC_I \tag{1}$$

$$Q(t) = A_Q \sin\left(\frac{4\pi x(t)}{\lambda} + \theta_0 + \Delta\phi\right) + DC_Q \tag{2}$$

where A_I and A_Q represent the amplitudes of the I/Q signals, respectively, $x(t)$ represents the displacement between the radar and human body surface, θ_0 denotes the absolute phase due to the initial distance between the subject and the system, $\triangle\phi$ is the I/Q phase imbalance, λ represents the wavelength of the carrier signal, DC_I and DC_Q are direct-current (DC) offsets for the I and Q channels, respectively. The displacement $x(t)$ between the radar and the surface of the human body (containing respiration, HS, and PW) can be assessed by the arctangent demodulation of the I/Q signals [24]. However, the amplitude and phase imbalance of the I/Q signals have to be calibrated and removed prior to the arctangent demodulation, which requires extra signal processing effort and increases complexity. As seen from (1) and (2), I/Q signals are modulated by displacement $x(t)$.Therefore, the HS and PW components are not physically separated at the receiver side, but can be extracted from the complex baseband I/Q signals during signal processing. Instead of explicitly reconstructing $x(t)$ using arctangent demodulation, we directly applied band-pass filtering to the I/Q signals to obtain HS- and PW-related components. A fourth-order Butterworth band-pass filter with passband of [16, 80] Hz is used to obtain the HS-related I/Q components [18], and a fourth-order Butterworth band-pass filter with passband of [0.67, 15] Hz is used to obtain the PW-related I/Q components, following prior CW radar studies [16], [17], [32] to improve separation between PW and HS bands. The filtered HS and PW I/Q signals were standardized within each segment using z-score standardization before being used as inputs to the network. Fig. 2 presents an example of the resulting HS and PW I/Q signals after per-segment z-score standardization. This standardization subtracts the segment mean and divides by the segment standard deviation, thereby reducing the influence of DC offset and amplitude-scale differences. Therefore, the displayed amplitudes are intended to emphasize waveform morphology and timing, rather than the raw amplitude relationship between HS and PW. The absolute amplitudes of the unstandardized bandpass signals can differ substantially between HS and PW and can vary across subjects and postures due to subject- and posture-dependent coupling in the bed-mounted measurement configuration, which changes the effective signal magnitude. In Fig. 2(a), a unified HS waveform is visible with the onset of the first heart sound (S1) well aligned with the R peak of the ECG. However, the PW I/Q from 1 s to 3 s shows a different pattern compared to the other segments, which may be influenced by respiratory motion. In Fig. 2(b), the HS I/Q signals exhibit a higher noise level, making the HS pattern less distinct, whereas a repetitive waveform remains visible in the PW I/Q signals. In addition, it is worth noticing that PW I/Q signals in Fig. 2(a) and Fig. 2(b) show different waveforms, which can be caused by the measured body position and vary between individuals [16]. Therefore, DL models are introduced to fuse heartbeat-related information from both HS and PW and to deal with the varying waveforms of signals.

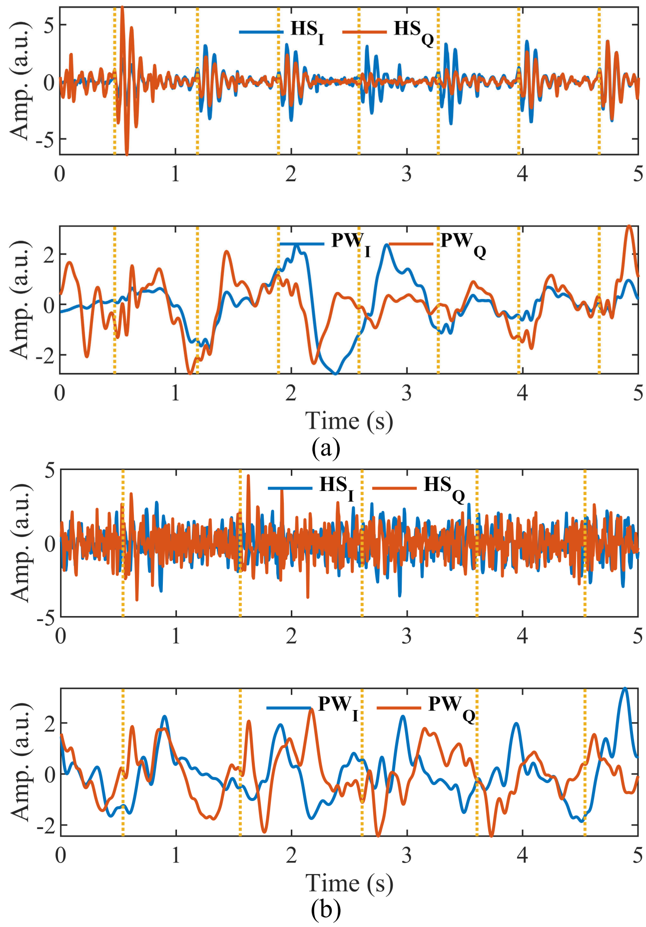

FIGURE 2. Exemplary HS and PW I/Q signals after z-score standardization within each segment. Yellow dashed line marks the timing of each R peak in ECG, representing heartbeat. (a) Clear waveform pattern in HS with inconsistent PW, and (b) noisy HS with a clear waveform pattern in PW.

B. MODEL OVERVIEW

Fig. 3 presents the proposed architectures of the fusion models, combining the information from HS and PW at different levels. The model architectures are described as follows:

- Data fusion (DataFu): HS and PW are concatenated as input for the feature model, fusing the information from HS and PW at the data level.
- Feature fusion (FeaFu): HS and PW are fed into the feature model separately. The extracted high-dimensional features are processed with dense layers and concatenated for the final prediction.
- Decision fusion (DecisionFu): HS and PW are input into the feature models separately. The prediction output of the HS and PW is averaged for the final prediction.
- Attention fusion (AttentionFu): HS and PW are input into the feature models separately. Thereafter, a self-attention module is individually applied to the output of the feature models, aligning the prediction within the same modality. Next, a cross-attention module is used to interact with the information from HS and PW.

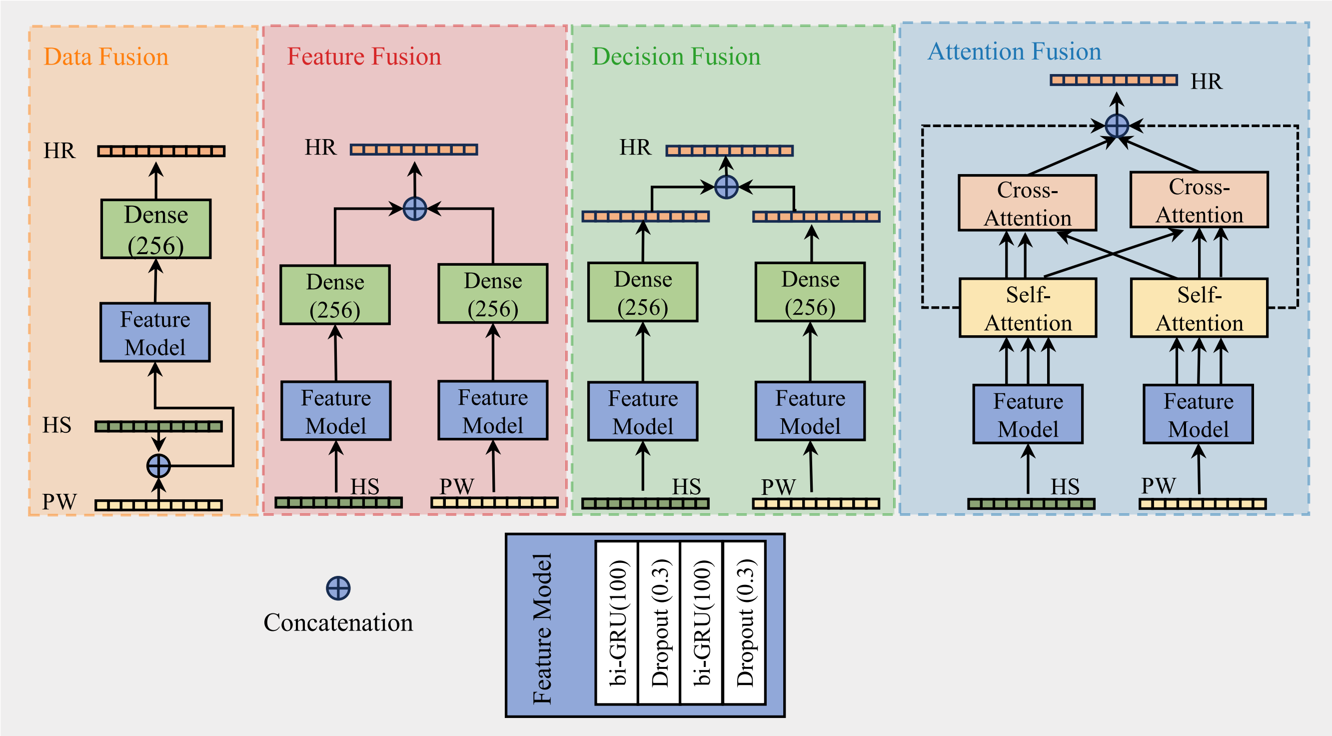

FIGURE 3. **Model architectures: data fusion, feature fusion, decision fusion, and attention fusion. The feature model extracts the high-dimension features from the HS and PW I/Q signals.**

The output of cross-attention and self-attention is concatenated for the final prediction.

The feature model and the self- and cross-attention modules are explained as follows.

1) FEATURE MODEL

As shown in Fig. 3, the feature model consists of two bi-GRU layers and two dropout layers. GRU (one of the RNN architectures) is suitable for capturing nonlinear temporal dependencies of a sequence. Bi-GRU combines the temporal dependencies captured from the forward and backward. Compared to LSTM, another type of RNN architecture, the GRU is simpler and contains fewer trainable parameters. In addition, GRU and LSTM have been used for radar-based heart sound detection with similar performance [20]. Therefore, in the feature model, bi-GRU is used to extract high-dimensional feature embedding from the HS and PW. In addition, the dropout layer is used to reduce overfitting during model training.

2) SELF- AND CROSS-ATTENTION

Self-attention was proposed by Vaswani et al. [30] and is widely used in different DL applications to integrate the information of the entire sequence to capture temporal correlations across different time frames formed by a weighted sum. In self-attention, high-dimensional features are projected into three different spaces: queries ($\mathbf{Q}$), keys ($\mathbf{K}$), and values ($\mathbf{V}$). The attention weights for each position of the sequence are calculated by applying a softmax function to the dot product of the $\mathbf{Q}$ and $\mathbf{K}$ matrices. Then, the attention weights are used to weight the $\mathbf{V}$ matrix and generate the weighted sum output. The self-attention module in the proposed AttentionFu method can be described as follows.

$$\mathbf{A}_{HS} = softmax\left(\mathbf{Q}_{HS}\mathbf{K}_{HS}^{T}\right) \tag{3}$$

$$\mathbf{A}_{PW} = softmax\left(\mathbf{Q}_{PW}\mathbf{K}_{PW}^{T}\right) \tag{4}$$

$$\text{SelfAttention}(HS) = \mathbf{A}_{HS}\mathbf{V}_{HS} \tag{5}$$

$$\text{SelfAttention}(PW) = \mathbf{A}_{PW}\mathbf{V}_{PW} \tag{6}$$

where $\mathbf{Q}_{HS}, \mathbf{K}_{HS}, \mathbf{V}_{HS}, \mathbf{Q}_{PW}, \mathbf{K}_{PW}, \mathbf{V}_{PW} \in \mathbb{R}^{L\times d}$ are projected from the feature model output of HS $\in \mathbb{R}^{L\times 2}$ and PW $\in \mathbb{R}^{L\times 2}$, respectively, with L denoting the number of time steps in the input radar signal segment and d representing the feature embedding dimensionality. $\mathbf{A}_{HS}$ and $\mathbf{A}_{PW} \in \mathbb{R}^{L\times L}$ represent the attention score of the HS and PW feature sequences, respectively.

To align the features of the HS and PW, cross-attention is proposed and can be described as follows.

$$\mathbf{A}_{(HS,PW)} = softmax\left(\mathbf{Q}_{PW}^{*}\mathbf{K}_{HS}^{*}\right) \tag{7}$$

$$\mathbf{A}_{(PW,HS)} = softmax\left(\mathbf{Q}_{HS}^{*}\mathbf{K}_{PW}^{*T}\right) \tag{8}$$

$$\text{CrossAttention}(HS, PW) = \mathbf{A}_{(HS,PW)}^{*}\mathbf{V}_{HS}^{*} \tag{9}$$

$$\text{CrossAttention}(PW, HS) = \mathbf{A}_{(PW,HS)}^{*}\mathbf{V}_{PW}^{*} \tag{10}$$

where $\mathbf{Q}^*_{HS}$, $\mathbf{K}^*_{HS}$, $\mathbf{V}^*_{HS}$, $\mathbf{Q}^*_{PW}$, $\mathbf{K}^*_{PW}$, $\mathbf{V}^*_{PW}$ $\in$ $\mathbb{R}^{L\times d^*}$ are projected from the outputs of the aforementioned self-attention modules (5) and (6).

Unlike self-attention, where the attention score is calculated as the dot product of the $\mathbf{Q}$ and $\mathbf{K}$ from the same modality, the attention score is computed by taking $\mathbf{Q}$ from one modality and $\mathbf{K}$ from another in cross-attention. $\mathbf{A}_{(HS,PW)}$ is determined using $\mathbf{K}^*_{HS}$ and $\mathbf{Q}^*_{PW}$, and helps align/fuse the features from HS and PW.

C. IBI ARTIFACT REMOVAL

IBI can be assessed by calculating the interval between two consecutive regular beats. Outliers in the IBI sequence can result in significant error in HRV parameter estimation, particularly in outlier-sensitive HRV parameters, e.g. those in the frequency domain. Therefore, outliers caused by extrasystole beats in reference ECG are detected using irregular changes in IBI [33] and visually controlled. Subsequently, the IBI from ECG are interpolated linearly to these positions. However, for IBI extracted from the radar system, outliers are mainly caused by false detections, e.g. missing (false negative) or additional (false positive) heartbeats. Therefore, IBI is filtered to remove outliers according to the method proposed by Vollmer et al. [33]. In addition, random body movement (RBM) may introduce large fluctuations into radar signals, resulting in false heartbeat detections and abnormal IBI values. To reduce the influence of RBM, a rule-based RBM detection method was applied before HRV analysis. First, the radar I/Q signals were filtered into the HS and PW frequency bands. Then, the mean amplitude and standard deviation of the filtered HS and PW I/Q signals were calculated within a two-second sliding window. Since RBM usually causes large and irregular amplitude variations, a segment was regarded as motion-contaminated when the mean amplitude or standard deviation exceeded predefined empirical thresholds. Heartbeat detections and IBI values located within these contaminated segments were excluded from subsequent IBI and HRV analysis. The thresholds are chosen empirically from the recorded data to distinguish segments with obvious movement artifacts (e.g., posture changes and large limb movements) from segments with normal cardiac and respiratory activity. The same thresholds were applied to all participants and body positions without subject-specific adjustment.

D. HRV PARAMETERS

HRV parameters are extracted in the time, frequency, and nonlinear domains. The HRV parameters are listed in Table 1.

E. PERFORMANCE EVALUATION

Performance is evaluated using metrics related to heartbeat detection, HR estimation, IBI analysis, and HRV assessment.

TABLE 1. Description of HRV parameters in time, frequency, and nonlinear domains [2].

HRV	Parameter	Description	Unit
Time domain	meanNN	average of the beat intervals	s
	SDNN	standard deviation of beat intervals	ms
	RMSSD	root mean square of successive difference	ms
	NN50	number of adjacent beat intervals difference higher than 50 ms	-
	TRI	area of histogram of NN intervals divided by its maximum height	-
	TINN	width of RR intervals histogram through triangular interpolation	-
Frequency domain	HF	power of high-frequency band [0.15, 0.4] Hz	-
	LF	power of low-frequency band [0.04, 0.15] Hz	-
	LF/HF	ratio of LF to HF	-
	pHF	HF normalized to the total power	-
	VLF	power of very low frequency band [0.0033, 0.04] Hz	-
Nonlinear domain	alpha1	short-term scaling exponent in detrended fluctuation analysis (DFA)	-
	alpha2	long-term scaling exponent in DFA	
	SD1	standard deviation of the distances perpendicular to the line of identity in the Poincaré plot	-
	SD2	standard deviation along the line of identity in the Poincaré Plot	-
	ApEn	approximate entropy	-
	SampEn	sample entropy	-

1) HEARTBEAT DETECTION

A tolerance range of 75 ms surrounding the ECG R peak is selected to determine the accuracy of heartbeat detection, which corresponds to half of the recognized tolerance range of 150 ms for ECG R-peak detection [34]. Specifically, a true positive (TP) is determined if the predicted heartbeat falls in this range. If no heartbeat is detected within the tolerance range, a false negative (FN) is counted. Conversely, a false positive (FP) is recorded if no R peak is found close to the radar-detected heartbeat. The performance metrics Sensitivity, Precision, and F1 score are defined as follows:

$$Sensitivity = \frac{TP}{TP + FN} \tag{11}$$

$$Precision = \frac{TP}{TP + FP} \tag{12}$$

$$F1 = \frac{2 * (Sensitivity * Precision)}{Sensitivity + Precision} \tag{13}$$

2) RELATIVE HR ERROR

The HR of the given windows from the radar and the ECG is calculated. Absolute relative HR error is defined as:

$$HR_{Error} = \frac{abs(HR_{Radar} - HR_{ECG})}{HR_{ECG}} \tag{14}$$

where the HR_{Radar} and HR_{ECG} represent the average HR within the specific window length detected by radar and ECG, respectively.

3) INTERBEAT INTERVAL (IBI)

The root mean square error (RMSE) of IBI by radar and ECG can be determined:

$$RMSE = \sqrt{\frac{\sum_{i=1}^{N}(IBI_{i,ECG} - IBI_{i,radar})^2}{N}} \tag{15}$$

4) HRV ERROR

Absolute relative HRV error can be determined as:

$$HRV_{Error}^{i} = \frac{abs(HRV_{Radar}^{i} - HRV_{ECG}^{i})}{HRV_{ECG}^{i}} \tag{16}$$

III. IMPLEMENTATION

A. DATASET

The dataset was collected at the *Medical University Lausitz – Carl Thiem* using the aforementioned 61 GHz CW radar system and *MP160* (*BIOPAC Systems, Inc., Goleta, CA 93117*) as the reference ECG system. A one-channel ECG was recorded to measure heart rate. The sampling frequencies of radar output and reference ECG were 8000 Hz and 4000 Hz, respectively. Radar I/Q signals and ECG signals were downsampled to 200 Hz. Importantly, the radar was not placed in front of the subject facing the chest. Instead, the radar system was mounted under the grid of a regular hospital bed, enabling sensing from below through the mattress with an approximate distance of 10 cm between the radar and the subject. Measurements were performed in different body positions: supine, left lateral, right lateral, and prone, while the radar placement remained unchanged across all postures. Initially, 37 minutes were recorded in the supine body position. In subsequent positions(left lateral, right lateral, and prone), each measurement was performed for another 5 minutes. A one-minute pause was given to alter the required positions. Overall, the recording duration was approximately one hour. Data were collected from 20 healthy subjects (11 males and 9 females, average age 43.05±14.64 years and BMI 27.59±5.14). Approximately 20 hours of data were collected. This study was approved by the ethics committee of Landesärztekammer Brandenburg (2023-40-MPDG-ff). All participants provided informed written consent prior to participation in accordance with ethical guidelines.

B. TRAINING DETAILS

Training and evaluation were performed on an HPC cluster using a single NVIDIA A100 GPU (40 GB) per job. The compute node is equipped with dual AMD EPYC 7662 CPUs (total 128 cores @ 2.0 GHz) and 512 GB RAM. The models were implemented in Python 3.9.23 using TensorFlow 2.10.0, and additional libraries include scikit-learn 1.3.0 for evaluation utilities.

5-fold cross-validation was conducted to evaluate performance. In each fold, data from 16 subjects were used for training and data from the remaining four subjects were used for evaluation. The models were implemented using *TensorFlow* [35]. During training, a mini-batch size of 48 and the early stopping of 5 epochs were used to reduce overfitting. The learning rate was set to 0.001, and the model was optimized using the *ADAM* [36] optimizer.

C. RUNTIME AND COMPUTATIONAL COST

To evaluate the computational cost and real-time feasibility of the proposed method, runtime was measured on the same HPC platform described above using a single NVIDIA A100 GPU. For the proposed models and fusion baselines, training was performed using the same five-fold cross-validation protocol. Since the models converged within 6-8 epochs across folds, we report the average training time per fold and the total training time over five folds. For testing, inference latency was measured with batch size of 1 using 5 s input windows. The reported inference time includes preprocessing and model inference for one input window. In addition, the number of trainable parameters is reported to characterize model complexity.

For reference, we also implemented a representative HS-based state-of-the-art method (HS-SOTA) following the method in [24]. However, HS-SOTA uses a 10 s window and a different preprocessing pipeline, which was originally performed in MATLAB. Therefore, its training time is not directly comparable with the proposed models and is not reported in the training time comparison. Instead, its number of trainable parameters and inference time are reported as reference values. Since many previous radar-based HR/HRV studies did not report training time or inference latency, a direct runtime comparison with prior studies is limited. Therefore, we report the measured runtime of all implemented methods and include the window length to indicate real-time feasibility.

As shown in Table 2, PW- and HS-based model have the same number of trainable parameters and very similar inference times, which is consistent with their identical network architecture. The small difference between them is marginal and can be attributed to normal runtime fluctuation in end-to-end latency measurement. DataFu has the same number of trainable parameters as PW- and HS-based model, but its inference time is higher because it uses both PW and HS inputs and therefore includes the preprocessing and input construction of both signal modalities. FeaFu and DecisionFu

TABLE 2. Computational cost and real-time feasibility (batch size=1).

Method	Params	Window (s)	Train time/fold (s)	Total train time (min)	Inference time (ms)
PW	295313	5	4514	376.2	142.29
HS	295313	5	3586	298.9	146.94
DataFu	296513	5	3148	262.4	163.38
FeaFu	590625	5	6250	520.85	186.98
DecisionFu	590626	5	8392	699.3	171.59
AttentionFu	656673	5	10356	862.7	189.22
HS-SOTA	2896004	10	-	-	159.78*

Note: For PW, HS, DataFu, FeaFu, DecisionFu, and AttentionFu, inference time includes preprocessing and model inference. *For HS-SOTA, only model inference time is reported; MATLAB-based preprocessing is not included.

have almost the same number of parameters, but FeaFu shows a higher inference time because feature-level fusion involves operations on intermediate feature representations, whereas decision-level fusion combines outputs directly. Therefore, inference time is not determined only by the number of trainable parameters, but also by the preprocessing cost, fusion strategy, and the type/shape of tensor operations involved in each model. Among all proposed fusion methods, AttentionFu has the largest number of parameters and the longest training time, but its inference time was only 189.22 ms for a 5 s input window, corresponding to less than 4% of the window duration. This indicates that the proposed AttentionFu method is computationally feasible for real-time HR and HRV monitoring. The HS-SOTA latency is reported only as a model-level reference because its MATLAB-based preprocessing was not included and its input window length differs from the proposed methods.

IV. RESULTS AND DISCUSSION

A. EFFECT OF THE WINDOW LENGTH

Fig. 4 shows the average F1 score of the proposed fusion methods and the single HS or PW model with a window length ranging from 1 s to 20 s. For all the models, with increasing window length, an initial increase in the average F1 score was observed followed by a subsequent decrease. Specifically, a short window length, e.g. one second, is not suitable for heartbeat detection. Given a resting heart rate of 60 bpm to 80 bpm, one second covers only one complete cardiac cycle, and with that the bi-GRU model cannot capture the information from adjacent beats. However, window lengths exceeding 10 s also resulted in a decrease in the performance of almost all models. This decrease in the model's performance associated with a long window length could be explained by the limitation of the bi-GRU model, which failed to handle long sequences even though the gated mechanism in the bi-GRU model helps to remember and forget the information from previous and following beats. In addition, models with a longer window are not preferred due to the extensive computation and memory demand, which limits the implementation on an edge device for real-time applications.

Comparing the HS-based- and PW-based models, the HS-based model showed superior performance. This could be explained by the relatively uniform wave-pattern of the HS signals. In contrast, the waveform of the PW depends on the body position and individual parameters of the subjects, thus increasing the inhomogeneity of the data. Among the fusion methods, AttentionFu achieved the best performance, followed by DataFu, for window lengths between 3 s and 10 s. Both AttentionFu and DataFu outperformed the HS and PW single models. A minor improvement was observed in the FeaFu model. No improvement could be achieved using the DecisionFu model.

In addition to our single-modality HS- and PW-based DL baselines and different fusion methods, we included

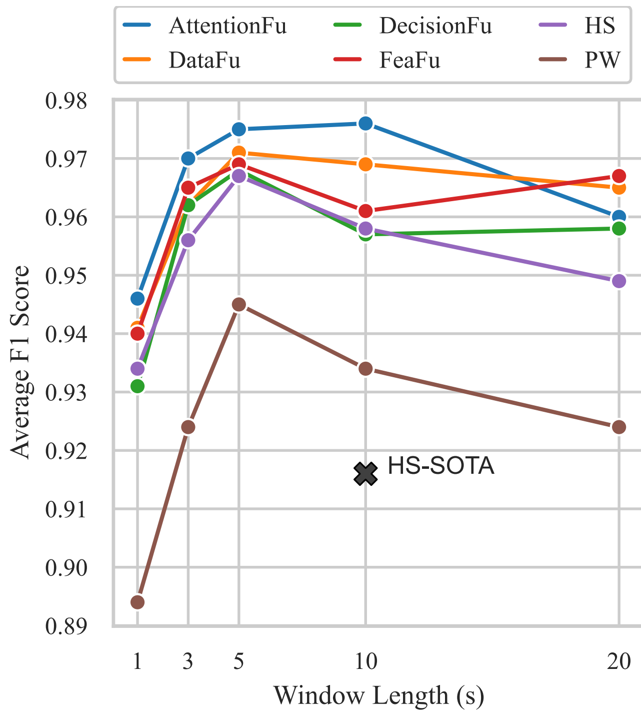

FIGURE 4. Comparison of the F1 score averaged over each measurement session across different window lengths and methods. AttentionFu, DecisionFu, FeaFu, and DataFu denote Attention Fusion, Decision Fusion, Feature Fusion, and Data Fusion, respectively. In addition, an HS-SOTA method from [24] is reported at its recommended 10 s window length (F1=0.916) and is therefore shown only at 10 s.

a representative HS-SOTA reported in [24]. Since the HS-SOTA method is designed for a 10 s window and relies on a specific preprocessing pipeline, we evaluated it under the same protocol and reported its performance at 10 s (F1=0.916) in Fig. 4. For comparison, at 10 s our HS-only DL baseline achieved and F1 score of 0.958 and the proposed AttentionFu achieved 0.976. Since the same input-window length was used, the performance difference between HS-SOTA and our HS-based model is not attributed to the window setting, but may be related to differences in preprocessing strategy, input representation, and network architecture. HS-SOTA uses a displacement-reconstruction-based preprocessing pipeline and a bidirectional LSTM network, whereas the our HS-based model uses filtered HS I/Q components within the same processing framework as the proposed fusion models. Therefore, HS-SOTA is included as a representative reference on the present dataset, rather than as a claim of general superiority over the HS-SOTA method. The results indicate that the filtered-I/Q HS representation is effective in the present framework, while AttentionFu further improves performance by adaptively fusing complementary HS and PW information. As shown in Fig. 4, most models achieved the best F1 scores with a window length of 5 s. Therefore, we use window length of 5 s in the following analyses and focus on methods implemented under a unified pipeline to ensure fair comparisons.

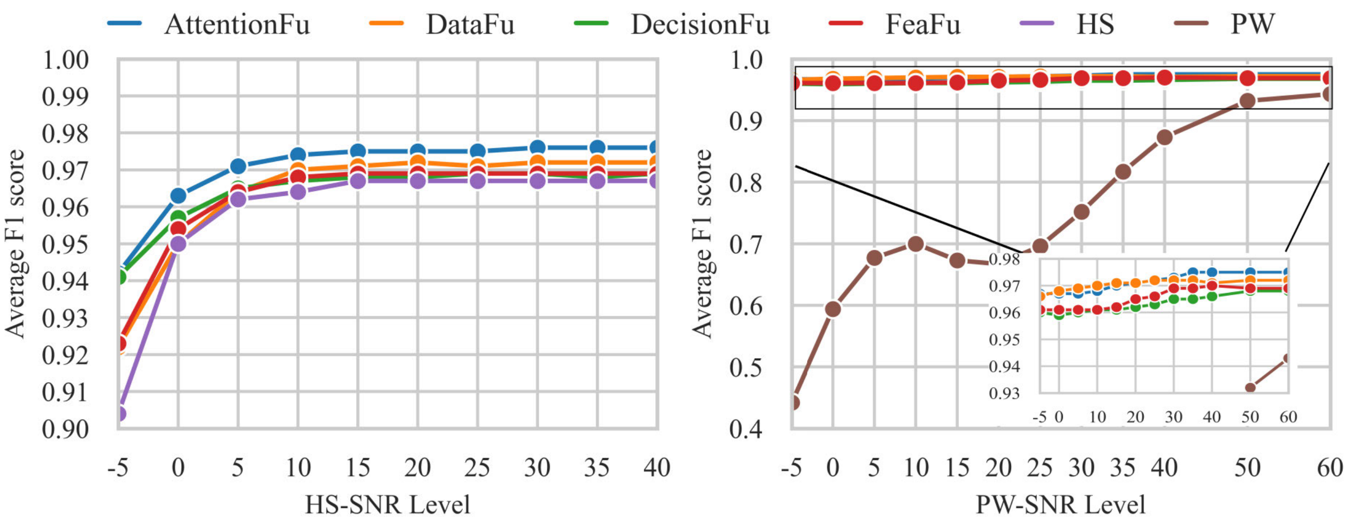

FIGURE 5. F1 score comparison across different SNR levels and methods. Left: noise added to HS I/Q signals; right: noise added to PW I/Q signals.

B. EFFECT OF BODY POSITIONS

Table 3 shows the performance of all the models with a window length of 5 s. The best performance was achieved in the prone and supine positions compared to the left and right-lateral positions. This could be explained by the lower signal quality in the lateral positions. AttentionFu performed best with sensitivity, precision and F1 scores ranging from 96% to 99% in all measured body positions. In contrast, DecisionFu failed to achieve higher performance than the HS model in the left lateral position. DecisionFu averaged the prediction output of the HS and PW, and misalignment between these predictions could result in FN or FP heartbeats, thus lowering sensitivity and precision. However, this misalignment can be addressed with the attention modules in the AttentionFu model.

TABLE 3. Heart Beat Detection Metrics comparison in different body positions.

Measured Body Position	Method	Sensitivity (%)	Precision (%)	F1 score (%)
Supine	PW	97.36±4.27	97.71±4.41	97.53±4.30
	HS	98.42±3.21	98.37±3.15	98.39±3.11
	DataFu	98.93±1.70	**98.90±2.03**	98.91±1.79
	FeaFu	98.53±2.82	98.57±2.75	98.54±2.70
	DecisionFu	98.72±1.82	98.61±2.20	98.66±1.88
	AttentionFu	**99.06±1.46**	98.88±2.09	**98.96±1.67**
Left Lateral	PW	90.55±13.37	92.53±11.23	91.51±12.33
	HS	94.95±10.15	96.10±7.21	95.48±8.80
	DataFu	95.38±10.39	96.28±7.78	95.79±9.19
	FeaFu	95.05±9.41	96.06±6.85	95.52±8.22
	DecisionFu	94.80±11.78	95.27±10.23	95.02±11.04
	AttentionFu	**95.79±9.41**	**96.32±7.60**	**96.04±8.55**
Right Lateral	PW	91.31±9.00	93.23±6.59	92.23±7.88
	HS	94.18±5.99	95.37±4.47	94.76±5.20
	DataFu	95.24±4.22	96.01±3.47	95.62±3.82
	FeaFu	95.03±4.65	96.32±3.35	95.66±3.97
	DecisionFu	95.15±4.91	95.92±3.64	95.52±4.21
	AttentionFu	**96.05±3.82**	**97.30±2.75**	**96.67±3.25**
Prone	PW	96.31±4.53	97.18±3.53	96.74±4.01
	HS	97.75±3.88	98.25±3.14	98.00±3.51
	DataFu	98.02±3.58	98.46±2.84	98.24±3.20
	FeaFu	97.73±3.74	98.26±3.29	97.99±3.47
	DecisionFu	97.91±3.40	98.27±2.58	98.08±2.97
	AttentionFu	**98.15±2.92**	**98.73±2.03**	**98.43±2.42**

C. EFFECT OF SNR LEVELS

Gaussian noise at varying levels was added directly to the HS and PW I/Q signals separately to investigate and evaluate the performance differences between the methods. The signal-to-noise ratio (SNR) is defined as follows:

$$SNR = 10 \log_{10} \left(\frac{\sum_{i=1}^{L} s_i^2}{\sum_{i=1}^{L} n_i^2} \right) \tag{17}$$

The average F1 score with varying SNR levels is shown in Fig. 5. With noise added to HS or PW, the average F1 score increased with improved SNR for all models. For HS in varying SNR levels, AttentionFu performed the best in comparison to the other fusion methods and the HS model. The difference between the fusion methods and the HS model decreased with increasing SNR. Comparing the F1 score for PW at different levels of SNR, similar improvements could be observed. The PW model was not robust to noise, whereas a higher F1 score could still be achieved with the HS model. The onset of S1 in the HS signal aligns well with the ECG R peak; however, this alignment is absent in the PW signal. Therefore, the addition of noise can shift the detected heartbeats from the PW signal, leading to a reduction in the accuracy of heartbeat detection. When comparing the same level of noise added to HS and PW I/Q signals, the fusion methods performed better if the noise was added to the PW rather than to the HS. This could be explained by the homogeneous waveform morphology of HS compared to PW [16], which was less affected by body position and individual differences. Therefore, fusion models tended to focus on HS rather than PW, resulting in a reduced impact on heartbeat detection when PW had a low SNR.

D. COMPARISON OF HR

AttentionFu showed a median relative HR error of 0.34%, outperforming the other fusion methods (0.38-0.55%, Fig. 6). In addition to the relative HR error, we compared the empirical cumulative distribution function (ECDF) of the absolute HR error, shown in Fig. 7. All methods showed similar performance within the HR error range of less than 1 bpm. With increasing HR error, the PW had the lowest ECDF, and DecisionFu showed an ECDF between the HS and PW models. In addition, AttentionFu ECDF was consistently higher than the other methods, indicating lower HR error. With AttentionFu, 95% of the data had an HR error of less than 5 bpm, and more than 97% of the data had an HR error of less than 10 bpm. These results highlighted the effectiveness of the proposed method with the CW radar system for contactless HR monitoring in different body positions.

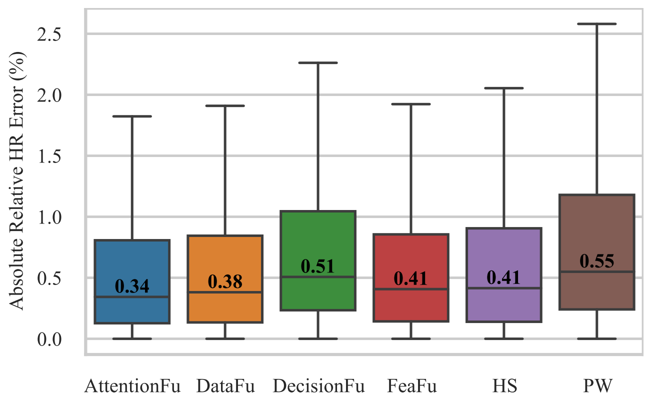

FIGURE 6. Boxplot of the absolute relative HR error.

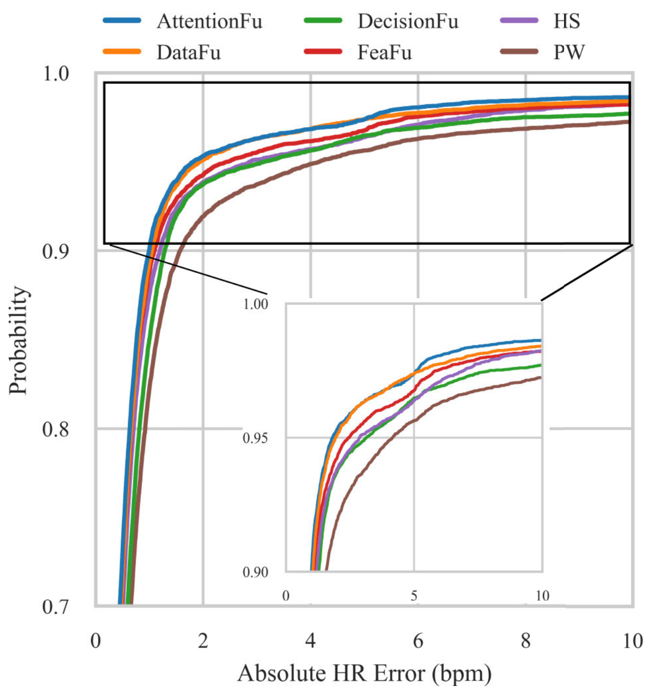

FIGURE 7. ECDF of absolute HR error.

E. COMPARISON OF INTERBEAT INTERVAL (IBI)

An example of IBI artifact removal using IBI filtering and RBM detection is shown in Fig. 8. In Fig. 8(a), one radar-derived beat was missed at approximately 150 s, producing a sudden IBI peak and increasing the IBI RMSE. After applying IBI filtering based on the relative change between consecutive IBIs, the abnormal IBI caused by the isolated missing beat was corrected by linear interpolation, leading to a reduced RMSE. This indicates that relative-change-based IBI filtering is effective for isolated IBI outliers caused by single missed beats. However, Fig. 8(b) shows a more challenging case in which the radar signals were contaminated by RBM, as highlighted in pink. During this interval, body movement caused continuous signal distortion and multiple missed or unreliable beat detections, resulting in abnormal IBI values. Although relative-change-based IBI filtering can correct isolated missing beats, it is insufficient for RBM-contaminated intervals because the corrupted IBIs are caused by sustained signal degradation rather than a single local outlier. Consequently, some movement-induced abnormal IBIs remained after IBI filtering alone, particularly near 215 s. The corresponding signal-level example of the RBM-contaminated segment from 200 to 215 s is provided in

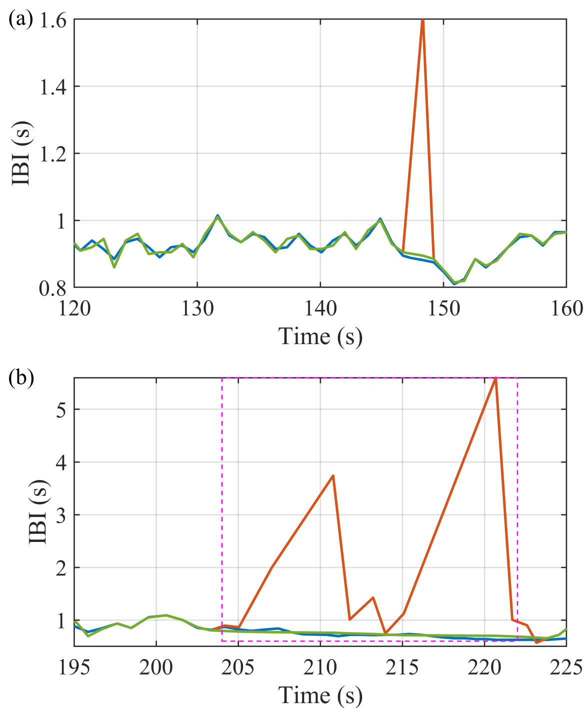

FIGURE 8. Example of IBI artifact removal with (a) filtering and (b) RBM detection. The blue line shows the IBI derived from ECG. The orange line represents the IBI from the radar before artifact removal, and the green line after artifact removal. The dashed pink box highlights the detected segment with RBM.

Appendix Fig. 10. As shown in Appendix Fig. 10, the filtered HS and PW I/Q signals exhibit sudden and pronounced amplitude fluctuations around 204-215 s. These abrupt amplitude changes correspond to the RBM-contaminated interval shown in Fig. 8(b), where missing radar-derived beats led to unrealistically high IBI values. After incorporating RBM detection, the movement-contaminated segment was identified and the corresponding abnormal IBI values were removed. This example demonstrates that combining IBI filtering with RBM detection is effective for suppressing IBI artifacts caused by both isolated missing beats and body movement.

The Pearson correlation coefficient (R), Bland-Altman bias, upper and lower limits of agreement (LOA), and RMSE of IBI between ECG and different methods with and without IBI artifact removal are summarized in Table 4. Without the removal of IBI artifacts, DecisionFu achieved the best performance, indicating fewer IBI outliers. Nevertheless, the performance of all methods without artifact removal was insufficient for reliable HRV estimation, because abnormal IBI values caused by missed or false heartbeat detections can strongly affect HRV parameters.

TABLE 4. Comparison of IBI Performance without (w/o) and with (w) IBI artifact removal.

Method	IBI artifact removal	R (%)	Bland-Altman			RMSE (ms)
			Bias (ms)	LOA (ms)		
PW	w/o	62.70	-14.68	-288.48	259.12	140.46
	w	92.20	-3.07	-97.62	91.48	48.34
HS	w/o	73.65	-6.64	-208.91	195.62	103.41
	w	94.78	-2.17	74.72	-79.06	39.29
DataFu	w/o	75.01	-5.62	-202.42	191.18	100.57
	w	96.59	-1.03	-62.79	60.73	31.53
FeaFu	w/o	74.45	-7.06	-207.30	193.19	102.41
	w	95.99	-1.62	-68.71	65.46	34.27
DecisionFu	w/o	79.39	-3.91	-173.19	165.37	86.46
	w	96.42	-1.49	-64.64	61.66	32.25
AttentionFu	w/o	72.50	-4.94	-213.88	203.99	106.71
	w	**97.11**	**-1.07**	**-57.85**	**55.71**	**28.99**

After IBI artifact removal, all parameters were substantially improved in all methods, and all fusion methods showed better results than the HS and PW models. An increase in correlation exceeding 15% and a high absolute correlation of more than 90% were achieved in all models, demonstrating the effectiveness of IBI artifact removal. Among all methods, AttentionFu achieves the best overall agreement with ECG after artifact removal, with the highest correlation coefficient of 97.11%, the lowest RMSE of 28.99 ms, and the narrowest Bland–Altman LOA from −57.85 ms to 55.71 ms. These results suggest that attention-based fusion provides more consistent beat-to-beat timing, which is important for subsequent HRV analysis.

The IBI derived from the ECG and from the radar system of all measurements was concatenated further agreement analysis. Using AttentionFu, a high R of 97.11% for IBI from ECG and radar was achieved after IBI artifact removal. However, the correlation could be affected by outliers and does not fully reflect the agreement between two measurement methods. Therefore, the Bland-Altman plot was used to visualize the agreement between both methods [37]. As shown in Fig. 9, the bias was only −1.07 ms, indicating minimal systematic disagreement between radar and ECG. The width of the upper and lower LOA were 55.71 ms and −57.85 ms, respectively. In addition, no linear trend was observed in the Bland-Altman plot, suggesting that the IBI estimation error was not strongly dependent on the mean IBI value.

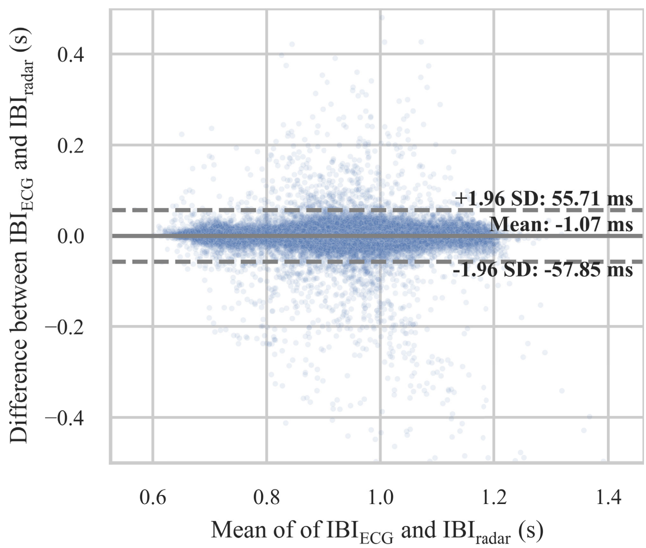

FIGURE 9. Bland-Altman plot of IBI from ECG and radar (AttentionFu with IBI artifact removal).

The superior performance of AttentionFu can be explained by the complementary characteristics of radar-derived HS and PW signals and the adaptive feature-level fusion ability of the attention mechanism. HS and PW are both related to cardiac activity, but they represent different physiological information. HS mainly reflects cardiac mechanical vibration, whereas PW reflects pulse-wave propagation on the body surface. Therefore, the two signals can provide complementary information for heartbeat detection and IBI estimation. However, their signal quality may vary across body positions, SNR levels, and measurement conditions. A fixed fusion strategy may therefore be insufficient to fully exploit their complementary information.

Different fusion strategies combine HS and PW information at different levels. DataFu performs input-level concatenation of HS and PW signals and feeds the concatenated signal into a shared feature extraction model. Although this strategy can use information from both modalities, the fusion is performed before modality-specific representations are fully learned. Therefore, noisy or unreliable components from one modality may affect the joint representation at an early stage. FeaFu extracts HS and PW features separately before concatenation, but the concatenation operation is still static and does not explicitly model the changing reliability of each modality. DecisionFu combines the outputs of independent HS and PW models only at the final decision level, which may limit the use of cross-modal information during feature learning.

In contrast, AttentionFu performs adaptive fusion at the feature-representation level. After modality-specific feature extraction, the attention modules allow the model to emphasize informative heartbeat-related features and suppress less reliable components. This is particularly useful for radar-based cardiac monitoring, because HS and PW may be affected differently by posture, noise, and local body-surface displacement. When one modality is degraded, the attention mechanism can reduce the contribution of less informative features and rely more on the complementary information from the other modality.

This interpretation is supported by both the HR error-distribution results in Fig. 7 and the IBI agreement results in Table 4. As shown in Fig. 7, AttentionFu achieved a slightly higher ECDF curve than DataFu, indicating a higher probability of obtaining smaller absolute HR errors. Consistently, Table 4 shows that AttentionFu achieved the highest correlation coefficient of 97.11%, compared with 96.59% for DataFu. The RMSE was reduced from 31.53 ms for DataFu to 28.99 ms for AttentionFu, corresponding to an approximate 8.1% relative reduction. In addition, the LOA range was reduced from 123.52 ms for DataFu to 113.56 ms for AttentionFu, suggesting improved agreement with the ECG reference. These results indicate that AttentionFu provides moderate but consistent improvements in HR error distribution, IBI estimation accuracy, and agreement with the ECG reference.

The benefit of AttentionFu is also reflected in the analyses under different body positions and SNR levels. Changes in body position and SNR level can affect the quality of HS and PW signals differently because the two components represent different physiological information related to cardiac activity. Therefore, the relative reliability of HS and PW is not fixed across all measurement conditions. The consistently high performance of AttentionFu in these analyses suggests that the attention-based fusion strategy can adapt to condition-dependent signal variations and provide more robust use of complementary HS and PW information.

F. HRV ASSESSMENT

1) HRV IN TIME, FREQUENCY, AND NONLINEAR DOMAINS

AttentionFu was selected for HRV assessment because it showed the best IBI estimation performance. HRV was extracted from the time, frequency, and nonlinear domain within a window size ranging from 60 s to 300 s. For each HRV parameter, the average absolute error, the average relative absolute error, the R between HRV detected by the ECG and the radar, and the Bland-Altman parameters were used as performance metrics. Appendix Table 6 summarizes the HRV performance metrics in the time domain. For meanNN, R of higher than 99% was achieved with AttentionFu for all HRV window lengths, and the performance improved with a longer window. For RMSSD and SDNN, absolute errors of 9.04 ms and 5.01ṁs were achieved with AttentionFu and a window length of 180 s, respectively. For NN50, a reduced absolute error was observed with shorter window length. By definition, NN50 analyses the total counts for adjacent beats exceeding 50 ms, and thus a higher cumulative absolute error would be expected for a longer window although the relative error remains unchanged. However, the relative error was not analyzed because the NN50 might be zero in some segments, leading to undefined relative error calculations (division by zero). For TRI, the lowest relative error of 14.04% with R of 91.10% was achieved with a window length of 300 s. The performance of TRI improved with window length, which could be explained by the increasing stability of the histogram distribution to calculate the TRI.

Appendix Table 7 summarizes the HRV performance in the frequency domain. For all given window lengths, all HRV parameters in the frequency domain were calculated with a relative error of less than 20% using AttentionFu. LF had a high R of 92.15%, and the relative error was less than 8%. Similar performance was achieved for the VLF. For HF, the relative error was higher compared to LF. For LF/HF, a relative error of 15.76% and a R of 75. 07% were achieved for a window length of 300 s. In the frequency domain, no trend of HRV could be observed with varying window lengths.

Appendix Table 8 shows the performance of HRV parameters in the nonlinear domain. For alpha1 and alpha2, low relative errors of 10.01% and 6.35% were achieved with a window length of 300 s, respectively. Notably, alpha2, which assesses long-term correlation in the series of RR intervals, showed improved performance with increasing window length. A longer window provides a more accurate assessment of long-term correlation by including more heart cycles and patterns that might influence heart rate in an extended period. Therefore, a longer window should be considered when analyzing alpha1 and alpha2. For SD1 and SD2, a high relative errors of 37.81% and 10.4% was achieved, respectively. A low absolute error was observed for both parameters. The numerical values of SD1 and SD2 are smaller than other nonlinear HRV parameters, with a median SD1 close to 0.025 and SD2 close to 0.05. A bias of 0.004 larger than zero could be observed, indicating that the radar system tended to estimate SD1 with higher values. SD1 analyzes the rapid beat-to-beat variability. Although the onset of radar S1 was found to be well aligned with the ECG R peaks, the detected onset of S1 could be slightly shifted within the tolerance range and reflected as fast beat-to-beat variability, contributing to a higher SD1. Our proposed method measured SD1 and SD2 with high correlation. The SD1, SD2 and SD1 / SD2 parameters have been proven to be useful for the identification of patients with atrial fibrillation [3], therefore, our proposed method may be a useful tool for monitoring those patients. For ApEn, the relative error decreased with window lengths. Windows of

TABLE 5. Comparison of radar-based HRV assessment with previous studies.

	Radar & Ref. System	Measurement	Signal	Method	HRV win. length [s] (sample size)	HRV Performance*: absolute error (relative error [%])						
						Time domain			Frequency Domain			
						SDNN [ms]	RMSSD [ms]	TRI (-)	LF (-)	HF (-)	LF/HF (-)	pHF (-)
Hu et al. [13]	2.4 GHz ECG	10 subjects; 40 minutes; sitting in labor	PW	EEMD	240 (10)	15.5 (19.99%)	2.5 (56.27%)	n.a.	30.21%	106.9%	n.a.	n.a.
Nosrati et al. [38]	2.4 GHz PPG	8 subjects; 40 minutes; sitting in labor	PW	frequency-time phase regression (FTPR)	300 (8)	9.57 (30.58%)	1.38 (39.46%)	n.a.	n.a.	n.a.	n.a.	n.a.
Petrovic et al. [15]	24 GHz ECG	10 subjects; 30 minutes; sitting in labor	PW	bandpass filter bank	180 (10)	1.97 (3.73%)	2.86 (8.41%)	n.a.	4.11%	17.5%	n.a.	n.a.
Yamamoto et al. [22]	24 GHz ECG	10 subjects; 120 minutes; sitting, talking, and typing in labor	PW	peak detection on the spectrogram	120 (60)	n.a.	n.a.	n.a.	n.a.	n.a.	median 3-5%	n.a.
Xie et al. [27]	24 GHz ECG	6 subjects; 60 minutes; sitting in labor	HS	decoding peak detection (DPD) and HSMM	300 (12)	2.37 (7.43%) 2.56 (8.53%)	7.06 (31.23%) 6.51 (29.30%)	n.a.	8.17% 11.75%	33.92% 18.1%	n.a.	n.a.
Shi et al. [24]	24 GHz *TFM* ECG	25 subjects; 350 minutes; cold fact test supine in clinical environment	HS	bi-LSTM	90 (260)	n.a.	n.a.	16.84%	10.25%	10.87%	11.15%	5.52%
Yen et al. [25]	24 GHz *BIOPAC* ECG	18 subjects; 36 minutes; supine without RBM in labor	PW	adaptive filtering	120 (18)	1.2 (2.64%)	3.7 (8.24%)	n.a.	3.32%	14.77%	n.a.	n.a.
Edanami et al. [26]	24 GHz *BIOPAC* ECG	9 subjects; 90 minutes; supine in labor; two neonates from NICU	PW	template matching	60 (90)	n.a.	n.a.	n.a.	R: 0.65	R: 0.79	n.a.	n.a.
Sameera et al. [28]	2.4 GHz PPG	4 subjects; 24 minutes; fixed breathing rate of 13, 15, 18 sitting in labor	PW	Peak Dection on MAMODWT, template matching	120 (12)	10.71 (28.32%)	14 (41.64%)	n.a.	n.a.	n.a.	n.a.	n.a.
This study	61 GHz *BIOPAC* ECG	20 subjects; approximate 1200 minutes; supine, left and right lateral, and prone in clinical environment	fusion of HS and PW	deep learning attention fusion	60-300 (200-1009)	Appendix Table A1 Nonlinear domain: Appendix Table A3			Appendix Table A2			

* HRV parameters, which were not compared in previous works are marked as n.a.

longer duration contain more IBI, leading to a stabilized and reliable estimation of ApEn. In addition, longer windows allow for the capture of more dynamic changes in the IBI, resulting in higher complexity and higher ApEn values. For SampEn, the recommended sample size is greater than 100 [1]. Therefore, the window lengths analyzed for SampEn were restricted to 120 s and 180 s. A favorable relative error was achieved for both entropy markers for a longer window, indicating that the radar system is able to capture the complexity of the ANS. In summary, a long window of 300 s is recommended to reliably measure nonlinear HRV parameters.

2) COMPARISON WITH PREVIOUS STUDIES

A summary of the comparisons with previous studies is presented in Table 5. To the best of our knowledge, this is the first study to assess HRV parameters using a CW system operating at 61 GHz. Previous studies have used CW radar systems operating at frequencies of 2.4 GHz or 24 GHz. A higher operating frequency allows a higher displacement resolution, thus improving the detection of HS components in micrometers. In addition, similar to [25] and [26], a clinical-certified *MP160 BIOPAC* system assessing the gold-standard ECG was introduced as a reference. In contrast, some studies relied on PPG [28], [38], which is less reliable for HR measurements.

Compared to recent studies [13], [15], [22], [26], [27], [28], [38] with a limited number of test subjects (less than 10), this study performed HRV measurements with extended duration with a larger cohort in varying body positions. In addition, the measurements were performed in a clinical setting rather than in a laboratory setting.

Whereas previous studies focused on either PW or HS, this study introduced the fusion of PW and HS using an attention-based DL model to improve the performance of HR and HRV monitoring. PW signals had been used to extract IBI by detecting the peaks by zero crossing after applying signal preprocessing techniques, e.g. filtering, template matching, and EEMD in [13], [15], [22], [25], [26], [28], and [38]. However, HS has been shown to be more robust for HR detection than PW, because HS has a more uniform pattern, is less dependent on measurement positions, and the onset of S1 is well aligned with the ECG R peak. Xie et al. [27] implemented a decoding peak detection (DPD) and HSMM model for HS detection and HRV estimation, and DPD and HSMM achieved similar performances. Shi et al. [19] performed HS-based segmentation with a DL model, bi-LSTM, which showed superior performance compared to the HSMM-based model. In this work, a bi-GRU model similar to bi-LSTM was implemented. We compared different DL-based fusion models and demonstrated that the fusion methods outperformed the HS- or PW-based methods.

Previous studies have limited HRV extraction to a single window length ranging from 60 s to 300 s, and the sample size of HRV segments ranged from 8 to 260. With a sample size of fewer than 20, HRV analysis may not provide reliable conclusions. Therefore, only three studies, [22], [24], [26], with a larger sample size were chosen to compare HRV performance using the same HRV window length. Higher R values of 82% and 88% for LF and HF were achieved in this work compared to those reported by Edanami et al. [26]. A low LF/HF error of 3% to 5% was achieved by Yamamoto and Ohtsuki [22], with only 10 subjects. Shi et al. [24] achieved a low relative error for HF, LF/HF, and pHF. However, we realized a lower error of 7.84%. In addition, TRI has been reported with an error of 16.84%, whereas we achieved a comparable value of 18.81%. Moreover, only the supine position was considered by Shi et al. [24], whereas we included the lateral positions, which exhibited worse signal quality than the supine position. In contrast to previous studies that focused on HRV estimation in the time or frequency domains, this work added an estimation of nonlinear HRV parameters, yielding promising results. With that, our model was able to measure the complexity and dynamics of IBI, showing great potential to assess the status of ANS for various clinical applications. In addition, we extracted HRV parameters using varying window lengths and compared the impact of window length on different HRV parameters, thereby providing a solid basis for comparison in future research.

One limitation of this study is that the robustness of the proposed method against RBM was not systematically evaluated using additional controlled body-movement experiments. Although the results before and after artifact removal demonstrate that excluding motion-contaminated segments improves IBI estimation performance, the current dataset does not support a detailed analysis of different RBM types, durations, or intensities. In addition, the artifact removal strategy uses empirical thresholds, which may require adjustment for different radar setups and measurement environments. Future work will include controlled and realistic body-movement conditions to collect dedicated motion-rich data and to develop adaptive or learning-based motion artifact detection methods. In addition, motion-aware modeling will be investigated to further improve the robustness of radar-based HR and HRV monitoring.

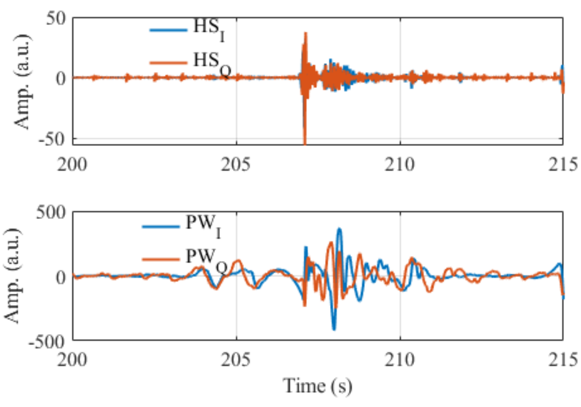

FIGURE 10. Example of filtered HS and PW I/Q signals in an RBM-contaminated segment from 200 to 215 s. This segment corresponds to the RBM interval shown in Fig. 8(b). Abrupt amplitude fluctuations are observed around 204–215,s in both HS and PW signals.

TABLE 6. Performance Metrics of HRV Assessment in the time domain.

HRV	Metrics	AttentionFu				
		60 s	90 s	120 s	180 s	300 s
meanNN	Error (ms)	2.60	2.44	2.42	2.03	**1.99**
	Error (%)	0.28	0.26	0.26	**0.21**	**0.21**
	R (%)	99.59	99.68	99.69	99.76	**99.82**
	Bias (ms)	1.08	1.08	1.13	**0.92**	1.23
	LOA (ms)	-18.41	-15.97	-15.70	-13.94	**-11.55**
		20.57	18.13	17.96	15.78	**14.01**
RMSSD	Error (ms)	9.69	9.62	9.49	**9.04**	9.65
	Error (%)	40.24	40.49	39.69	**37.80**	39.56
	R (%)	86.95	87.67	88.32	**90.65**	89.09
	Bias (ms)	6.23	6.34	6.27	**5.83**	6.75
	LOA (ms)	-22.53	-21.28	-20.73	-18.90	**-18.73**
		35.00	33.95	33.26	**30.56**	32.23
SDNN	Error (ms)	5.67	5.60	5.51	**5.01**	5.42
	Error (%)	17.52	16.41	15.94	**13.78**	14.53
	R (%)	85.12	85.57	86.16	**89.14**	87.87
	Bias (ms)	3.18	3.21	3.12	**2.72**	3.41
	LOA (ms)	-23.15	-22.55	-22.46	**-19.17**	-20.25
		29.50	28.97	28.70	**24.60**	27.08
NN50	Error (-)	**4.29**	6.20	8.05	11.30	19.56
	R (%)	90.06	90.92	91.61	**93.16**	92.61
	Bias (-)	**2.84**	4.22	5.52	7.65	14.30
	LOA (-)	**-8.46**	-11.86	-15.18	-21.17	-33.66
		14.14	20.30	26.21	36.47	62.26
TRI	Error (-)	1.48	1.42	1.36	1.39	**1.34**
	Error (%)	21.11	18.81	16.87	16.07	**14.04**
	R (%)	74.10	81.61	84.88	87.10	**91.10**
	Bias (-)	**0.27**	0.31	0.24	0.40	0.55
	LOA (-)	-3.77	-3.44	-3.45	-3.28	**-3.03**
		4.31	4.06	**3.94**	4.09	4.13

TABLE 7. Performance Metrics of HRV Assessment in the frequency domain.

HRV	Metrics	AttentionFu				
		60 s	90 s	120 s	180 s	300 s
HF	Error (-)	**0.40**	0.68	0.56	0.91	0.68
	Error (%)	**17.97**	18.77	18.73	19.00	19.04
	R (%)	82.48	80.81	81.18	82.73	**82.74**
	Bias (-)	**0.27**	0.48	0.41	0.67	0.54
	LOA (-)	**-0.82**	-1.31	-1.09	-1.62	-1.14
		1.37	2.28	1.92	2.97	2.22
LF	Error (-)	**0.18**	0.28	0.21	0.32	0.24
	Error (%)	7.13	6.94	6.16	**5.57**	6.14
	R (%)	88.57	89.35	90.96	91.75	**92.15**
	Bias (-)	-0.05	-0.07	-0.05	-0.07	**-0.01**
	LOA (-)	**-0.67**	-0.99	-0.74	-1.05	-0.75
		0.56	0.85	**0.64**	0.91	0.72
LF/HF	Error (-)	0.21	0.21	0.21	**0.2**	**0.2**
	Error (%)	17.57	17.44	16.66	15.93	**15.76**
	R (%)	**76.6**	73.74	72.51	75.46	75.07
	Bias (-)	**-0.15**	**-0.15**	**-0.15**	-0.16	**-0.15**
	LOA (-)	-0.8	-0.78	-0.78	-0.74	**-0.72**
		0.5	0.48	0.47	0.42	**0.41**
pHF	Error (-)	4.73	4.78	4.6	4.49	**4.4**
	Error (%)	10.93	10.92	10.66	10.41	**10.2**
	R (%)	83.96	82.47	82.25	83.59	**84.71**
	Bias (-)	**3.06**	3.19	3.17	3.32	3.2
	LOA (-)	-10	-9.78	-9.39	-8.34	**-8.04**
		16.13	16.17	15.72	14.99	**14.44**
VLF	Error (-)	**0.13**	0.2	0.16	0.26	0.2
	Error (%)	10.18	8.86	7.93	7.05	**6.9**
	R (%)	88.75	**88.86**	88.26	87.76	87.12
	Bias (-)	**-0.05**	-0.1	-0.08	-0.12	-0.09
	LOA (-)	**-0.49**	-0.73	-0.6	-0.93	-0.67
		0.38	0.54	0.44	0.68	0.48

TABLE 8. Performance Metrics of HRV Assessment in the nonlinear domain.

HRV	Metrics	AttentionFu				
		60 s	90 s	120 s	180 s	300 s
alpha1	Error (-)	0.117	0.115	0.114	0.11	**0.102**
	Error (%)	12.33	11.89	11.35	10.85	**10.01**
	R (%)	82.77	81.91	80.54	82.12	**83.73**
	Bias (-)	-0.075	-0.073	-0.076	-0.076	**-0.07**
	LOA (-)	-0.406	-0.387	-0.393	-0.365	**-0.339**
		0.257	0.241	0.24	0.212	**0.199**
alpha2	Error (-)	0.064	0.064	0.055	0.053	**0.052**
	Error (%)	13.13	10.93	8	7.11	**6.35**
	R (%)	**93.33**	90.39	92.85	92.16	91.82
	Bias (-)	**-0.015**	-0.02	-0.021	-0.022	-0.026
	LOA ()	-0.275	-0.278	-0.226	-0.204	**-0.188**
		0.246	0.238	0.185	0.159	**0.136**
SD1	Error (-)	0.007	0.007	0.007	**0.006**	0.007
	Error (%)	40.29	40.52	39.7	**37.81**	39.56
	R (%)	86.94	87.67	88.32	**90.65**	89.09
	Bias (-)	**0.004**	**0.004**	**0.004**	**0.004**	0.005
	LOA (-)	-0.016	-0.015	-0.015	**-0.013**	**-0.013**
		0.025	0.024	0.024	**0.022**	0.023
SD2	Error (-)	0.006	0.006	0.006	**0.005**	0.006
	Error (%)	13.64	12.57	12.52	**10.44**	11.01
	R (%)	84.11	84.63	85.2	**88.26**	87.46
	Bias (-)	0.003	0.003	0.003	**0.002**	0.003
	LOA (-)	-0.031	-0.03	-0.03	**-0.025**	-0.027
		0.037	0.036	0.036	**0.03**	0.033
SD1/SD2	Error (-)	0.11	0.108	0.103	0.097	**0.095**
	Error (%)	27.73	28.36	28.05	**26.96**	27.36
	R (%)	71.95	71.6	71.59	72.74	**72.91**
	Bias (-)	0.085	0.085	0.082	**0.078**	**0.078**
	LOA (-)	-0.203	-0.195	-0.184	-0.167	**-0.158**
		0.372	0.365	0.347	0.324	**0.313**
ApEn	Error (-)	0.116	0.113	0.104	**0.099**	**0.099**
	Error (%)	36.74	23.2	18.07	12.77	**10.93**
	R (%)	40.21	41.28	**41.68**	35.1	20.7
	Bias (-)	-0.01	-0.004	**0.003**	0.014	0.04
	LOA (-)	-0.328	-0.323	-0.302	-0.28	**-0.255**
		0.308	0.314	**0.307**	0.308	0.336
SampEn	Error (-)	-	-	-	0.271	**0.251**
	Error (%)	-	-	-	17.42	**16.45**
	R (%)	-	-	-	47.03	**45.53**
	Bias (-)	-	-	-	0.062	**0.06**
	LOA (-)	-	-	-	-0.668	**-0.614**
		-	-	-	0.791	**0.735**

V. CONCLUSION

In this study, we demonstrated that fusion of HS- and PW-related radar signals can improve the quality of heartbeat-related information obtained from a CW radar system. Compared with single-modality and other fusion baselines, the proposed attention-based fusion method (AttentionFu) provided moderate but consistent improvements in HR and IBI estimation, while maintaining real-time feasibility. In combination with automatic IBI artifact removal, AttentionFu achieved an F1 score exceeding 97% for contactless heartbeat detection and showed the best overall performance for HRV assessment in time, frequency, and nonlinear domains across different body positions. These results indicate that adaptive fusion of complementary HS and PW information is a promising strategy for radar-based HR and HRV monitoring. Further studies are needed to evaluate the robustness of the method under controlled body-movement conditions and to investigate its suitability in cohorts with cardiovascular disease.

APPENDIX

See Fig. 10 and Tables 6–8.

REFERENCES

[1] T. F. O. T. E. S. O. C. T. N. A. S. O. P. Electrophysiology, "Heart rate variability: Standards of measurement, physiological interpretation, and clinical use," *Circulation*, vol. 93, no. 5, pp. 1043–1065, 1996.

[2] F. Shaffer and J. P. Ginsberg, "An overview of heart rate variability metrics and norms," *Frontiers Public Health*, vol. 5, Sep. 2017, Art. no. 290215.

[3] Z. Mei, X. Gu, H. Chen, and W. Chen, "Automatic atrial fibrillation detection based on heart rate variability and spectral features," *IEEE Access*, vol. 6, pp. 53566–53575, 2018.

[4] C. Schiweck, D. Piette, D. Berckmans, S. Claes, and E. Vrieze, "Heart rate and high frequency heart rate variability during stress as biomarker for clinical depression. A systematic review," *Psychol. Med.*, vol. 49, no. 2, pp. 200–211, Jan. 2019.

[5] G. Matar, J.-M. Lina, J. Carrier, and G. Kaddoum, "Unobtrusive sleep monitoring using cardiac, breathing and movements activities: An exhaustive review," *IEEE Access*, vol. 6, pp. 45129–45152, 2018.

[6] J. Jeppesen, A. Fuglsang-Frederiksen, P. Johansen, J. Christensen, S. Wüstenhagen, H. Tankisi, E. Qerama, A. Hess, and S. Beniczky, "Seizure detection based on heart rate variability using a wearable electrocardiography device," *Epilepsia*, vol. 60, no. 10, pp. 2105–2113, Oct. 2019.

[7] J. Tu and J. Lin, "Fast acquisition of heart rate in noncontact vital sign radar measurement using time-window-variation technique," *IEEE Trans. Instrum. Meas.*, vol. 65, no. 1, pp. 112–122, Jan. 2016.

[8] Q. Lv, L. Min, C. Cao, S. Zhou, D. Zhou, C. Zhu, Y. Li, Z. Zhu, X. Li, and L. Ran, "Time-domain Doppler biomotion detections immune to unavoidable DC offsets," *IEEE Trans. Instrum. Meas.*, vol. 70, pp. 1–10, 2021.

[9] X. Chen and X. Ni, "Noncontact sleeping heartrate monitoring method using continuous-wave Doppler radar based on the difference quadratic sum demodulation and search algorithm," *Sensors*, vol. 22, no. 19, p. 7646, Oct. 2022.

[10] M. Li and J. Lin, "Wavelet-transform-based data-length-variation technique for fast heart rate detection using 5.8-GHz CW Doppler radar," *IEEE Trans. Microw. Theory Techn.*, vol. 66, no. 1, pp. 568–576, Jan. 2018.

[11] J. Park, J.-W. Ham, S. Park, D.-H. Kim, S.-J. Park, H. Kang, and S.-O. Park, "Polyphase-basis discrete cosine transform for real-time measurement of heart rate with CW Doppler radar," *IEEE Trans. Microw. Theory Techn.*, vol. 66, no. 3, pp. 1644–1659, Mar. 2018.

[12] J.-Y. Shih and F.-K. Wang, "Quadrature cosine transform (QCT) with varying window length (VWL) technique for noncontact vital sign monitoring using a continuous-wave (CW) radar," *IEEE Trans. Microw. Theory Techn.*, vol. 70, no. 3, pp. 1639–1650, Mar. 2022.

[13] W. Hu, Z. Zhao, Y. Wang, H. Zhang, and F. Lin, "Noncontact accurate measurement of cardiopulmonary activity using a compact quadrature Doppler radar sensor," *IEEE Trans. Biomed. Eng.*, vol. 61, no. 3, pp. 725–735, Mar. 2014.

[14] F. E. Churchill, G. W. Ogar, and B. J. Thompson, "The correction of I and Q errors in a coherent processor," *IEEE Trans. Aerosp. Electron. Syst.*, vols. AES–17, no. 1, pp. 131–137, Jan. 1981.

[15] V. L. Petrovic, M. M. Jankovic, A. V. Lupšic, V. R. Mihajlovic, and J. S. Popovic-Božovic, "High-accuracy real-time monitoring of heart rate variability using 24 GHz continuous-wave Doppler radar," *IEEE Access*, vol. 7, pp. 74721–74733, 2019.

[16] C. Will, K. Shi, S. Schellenberger, T. Steigleder, F. Michler, R. Weigel, C. Ostgathe, and A. Koelpin, "Local pulse wave detection using continuous wave radar systems," *IEEE J. Electromagn., RF Microw. Med. Biol.*, vol. 1, no. 2, pp. 81–89, Dec. 2017.

[17] C. Will, K. Shi, R. Weigel, and A. Koelpin, "Advanced template matching algorithm for instantaneous heartbeat detection using continuous wave radar systems," in *IEEE MTT-S Int. Microw. Symp. Dig.*, May 2017, pp. 1–4.

[18] C. Will, K. Shi, S. Schellenberger, T. Steigleder, F. Michler, J. Fuchs, R. Weigel, C. Ostgathe, and A. Koelpin, "Radar-based heart sound detection," *Sci. Rep.*, vol. 8, no. 1, p. 11551, Jul. 2018.

[19] K. Shi, S. Schellenberger, F. Michler, T. Steigleder, A. Malessa, F. Lurz, C. Ostgathe, R. Weigel, and A. Koelpin, "Automatic signal quality index determination of radar-recorded heart sound signals using ensemble classification," *IEEE Trans. Biomed. Eng.*, vol. 67, no. 3, pp. 773–785, Mar. 2020.

[20] H. Lu, M. Heyder, M. Wenzel, N. C. Albrecht, D. Langer, and A. Koelpin, "Accurate heart beat detection with Doppler radar using bidirectional GRU network," in *Proc. IEEE Radio Wireless Symp. (RWS)*, Jan. 2023, pp. 52–54.

[21] N. Malešević, V. Petrović, M. Belić, C. Antfolk, V. Mihajlović, and M. Janković, "Contactless real-time heartbeat detection via 24 GHz continuous-wave Doppler radar using artificial neural networks," *Sensors*, vol. 20, no. 8, p. 2351, Apr. 2020.

[22] K. Yamamoto and T. Ohtsuki, "Non-contact heartbeat detection by heartbeat signal reconstruction based on spectrogram analysis with convolutional LSTM," *IEEE Access*, vol. 8, pp. 123603–123613, 2020.

[23] K. Shi, S. Schellenberger, L. Weber, J. P. Wiedemann, F. Michler, T. Steigleder, A. Malessa, F. Lurz, C. Ostgathe, R. Weigel, and A. Koelpin, "Segmentation of radar-recorded heart sound signals using bidirectional LSTM networks," in *Proc. 41st Annu. Int. Conf. IEEE Eng. Med. Biol. Soc. (EMBC)*, Jul. 2019, pp. 6677–6680.

[24] K. Shi, T. Steigleder, S. Schellenberger, F. Michler, A. Malessa, F. Lurz, N. Rohleder, C. Ostgathe, R. Weigel, and A. Koelpin, "Contactless analysis of heart rate variability during cold pressor test using radar interferometry and bidirectional LSTM networks," *Sci. Rep.*, vol. 11, no. 1, p. 3025, Feb. 2021.

[25] H. T. Yen, M. Kurosawa, T. Kirimoto, Y. Hakozaki, T. Matsui, and G. Sun, "Non-contact estimation of cardiac inter-beat interval and heart rate variability using time-frequency domain analysis for CW radar," *IEEE J. Electromagn., RF Microw. Med. Biol.*, vol. 7, no. 4, pp. 457–467, Dec. 2023.

[26] K. Edanami, M. Kurosawa, H. T. Yen, T. Kanazawa, Y. Abe, T. Kirimoto, Y. Yao, T. Matsui, and G. Sun, "Remote sensing of vital signs by medical radar time-series signal using cardiac peak extraction and adaptive peak detection algorithm: Performance validation on healthy adults and application to neonatal monitoring at an NICU," *Comput. Methods Programs Biomed.*, vol. 226, Nov. 2022, Art. no. 107163.

[27] Z. Xie, H. Wang, S. Han, E. Schoenfeld, and F. Ye, "DeepVS: A deep learning approach for RF-based vital signs sensing," in *Proc. 13th ACM Int. Conf. Bioinf., Comput. Biol. Health Informat.*, Aug. 2022, pp. 1–5.

[28] J. N. Sameera, M. S. Ishrak, V. M. Lubecke, and O. Boric-Lubecke, "Enhancing beat-to-beat analysis of heart signals with respiration harmonics reduction through demodulation and template matching," *IEEE Trans. Microw. Theory Techn.*, vol. 72, no. 1, pp. 750–758, Jan. 2024.

[29] K. Holldack and D. Wolf, *Atlas und kurzgefaßtes lehrbuch der phonokardiographie und verwandter untersuchungsmethoden*. Stuttgart, Germany: Thieme, 1966.

[30] A. Vaswani, N. Shazeer, N. Parmar, J. Uszkoreit, L. Jones, A. N. Gomez, Ł. Kaiser, and I. Polosukhin, "Attention is all you need," in *Proc. Adv. Neural Inf. Process. Syst.*, vol. 30, 2017, pp. 5998–6008.

[31] R. Holzschuh, R. Freund, S. Ortmann, H. Lu, B. Sutbas, A. Bezer, and D. Große Meininghaus, "Contactless assessment of physiological parameters with a 61 GHz CW medical radar system, "Contactless assessment of physiological parameters with a 61 GHz CW medical radar system," in *Proc. iCCC-iCampμs Cottbus Conf.*, 2024, pp. 53–57.

[32] S. Schellenberger, K. Shi, T. Steigleder, A. Malessa, F. Michler, L. Hameyer, N. Neumann, F. Lurz, R. Weigel, C. Ostgathe, and A. Koelpin, "A dataset of clinically recorded radar vital signs with synchronised reference sensor signals," *Sci. Data*, vol. 7, no. 1, p. 291, Sep. 2020.

[33] M. Vollmer, "A robust, simple and reliable measure of heart rate variability using relative RR intervals," in *Proc. Comput. Cardiol. Conf. (CinC)*, Sep. 2015, pp. 609–612.

[34] *Testing and Reporting Performance Results of Cardiac Rhythm and St Segment Measurement Algorithms*, Standard ANSI/AAMI EC57, 2012.

[35] M. Abadi, A. Barham, J. Chen, Z. Chen, A. Davis, J. Dean, M. Devin, S. Ghemawat, G. Irving, M. Isard, M. Kudlur, J. Levenberg, R. Monga, S. Moore, D. G. Murray, B. Steiner, P. Tucker, V. Vasudevan, P. Warden, M. Wicke, Y. Yu, and X. Zheng, "TensorFlow: A system for large-scale machine learning," in *Proc. 12th USENIX Symp. Operating Syst. Des. Implement. (OSDI)*, Savannah, GA, USA, 2016, pp. 265–283.

[36] D. P. Kingma and J. Ba, "Adam: A method for stochastic optimization," 2014, *arXiv:1412.6980*.

[37] J. M. Bland and D. Altman, "Statistical methods for assessing agreement between two methods of clinical measurement," *Lancet*, vol. 327, no. 8476, pp. 307–310, 1986.

[38] M. Nosrati and N. Tavassolian, "High-accuracy heart rate variability monitoring using Doppler radar based on Gaussian pulse train modeling and FTPR algorithm," *IEEE Trans. Microw. Theory Techn.*, vol. 66, no. 1, pp. 556–567, Jan. 2018.

HUI LU (Member, IEEE) received the M.Sc. degree in mechanical engineering from RWTH Aachen University, Germany, in 2019. She is currently pursuing the Ph.D. degree with the Institute of High-Frequency Technology, Hamburg University of Technology, Hamburg, Germany.

Her current research interests include radar signal processing, deep learning for biomedical applications, and autonomous driving. She has authored or co-authored more than ten publications in her areas of interest. She serves as a Reviewer for IEEE Microwave and Wireless Technology Letters.

ROBERT HOLZSCHUH received the Dipl.-Ing. degree in medical engineering from Berufsakademie Sachsen, Staatliche Studienakademie Bautzen, Germany, in 2011. From 2008 to 2021, he held various technical and managerial positions in medical device development, quality management, and global research and development at GML AG, D.Med Consulting GmbH, and Fresenius Medical Care. Since 2022, he has been a Scientific Project Manager for Medical Technology Development with Thiem-Research GmbH, Cottbus, Germany, where he leads research and development projects, clinical investigations, and technology transfer activities. His research interests include medical device development, clinical evaluation, optical data transmission, and innovation processes in healthcare.

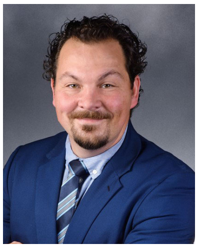

ROBERT FREUND received the Diploma degree in molecular biotechnology from Bielefeld University, Bielefeld, Germany, in 2008, and the Dr. rer. nat. degree in biochemistry from Hannover Medical School (MHH), Hanover, Germany, in 2014, where he studied molecular signal transduction in skeletal and cardiac muscle.

From 2014 to 2019, he was a Postdoctoral Researcher with MHH, followed by a Postdoctoral position with the Federal Institute for Materials Research and Testing (BAM), where he worked on digitization in the quality infrastructure. From 2021 to 2025, he was a Scientific Project Lead with Thiem-Research GmbH, coordinating clinical studies and digital-health projects within the Medical Informatics Initiative (MII) and the Network of University Medicine (NUM). In 2025, he joined Medical University Lausitz–Carl Thiem, where he first headed the Scientific Advisory and is currently the Head of the Core Units and Research Services, responsible for research coordination, research infrastructure and services, biobanking, and science communication. He has co-authored several peer-reviewed publications and conference papers in cardiology, electrophysiology, telemedicine, and medical technology. His research interests include digital health infrastructures, cardiovascular risk identification, biosignal processing, clinical research management, and AI-supported medical technologies.

Dr. Freund is a member of national scientific consortia within the MII and NUM.

STEFFEN ORTMANN received the Diploma degree in computer science and the Ph.D. degree in engineering.

From 2019 to 2025, he established and the Head of Thiem-Research GmbH, a 100% research-subsidiary of a large community hospital in Cottbus, Germany, where he is also coordinating the science activities. Before that, he gathered more than 15 years of experience in leading national and European mHealth and eHealth research projects in a non-university research institute. He is currently the Head of science coordination and new business areas with Munich Municipal Hospital Group, focusing on innovative telemedicine and artificial intelligence. He is with the Department of Operative Hospital Management, München Klinik gGmbH, Munich, Germany. He has published more than 60 refereed technical articles about wearables and medical sensors, mHealth applications, and the implementation of concepts and applications in telemedicine. His research interests include medical wearables, infrastructure for tele-medical innovations, eHealth, and the digital hospital.

DIRK GROSSE MEININGHAUS is currently the Director of the Department of Cardiology and a Professor with the Cardiovascular Health Services Research, Medical University Lausitz–Carl Thiem, Cottbus, Germany. He completed Medical School, in 1993, and received training in cardiology and electrophysiology in Hamburg and Bremen, Germany. His special research interests include catheter ablation of arrhythmias, atrial fibrillation, heart failure, cardiac resynchronization therapy, as well as health services research and health economics.

ALEXANDER KOELPIN (Fellow, IEEE) received the Diploma degree in electrical engineering and the Ph.D. and Habilitation degrees from the Friedrich-Alexander University of Erlangen–Nuremberg (FAU), Germany, in 2005, 2010, and 2014, respectively.

From 2005 to May 2017, he was with the Institute for Electronics Engineering, FAU. From 2007 to 2010, he was a Team Leader. From 2010 to 2015, he was a Group Leader Circuits, Systems and Hardware Test. Since 2015, he has been a Leader of the Electronic Systems Group. From June 2017 to February 2020, he was a Professor and the Head of the Chair for Electronics and Sensor Systems, Brandenburg University of Technology Cottbus–Senftenberg, Germany. Since March 2020, he has been a Professor with Hamburg University of Technology, Germany, and the Head of the Institute of High-Frequency Technology. His research interests include microwave circuits and systems, radar and wireless sensing, wireless communication systems, local positioning, and six-port technology. He has authored or co-authored more than 300 publications in his areas of interest.

Dr. Koelpin is a member of the Commission A: Electromagnetic Metrology of U.R.S.I. Since 2016, he has been awarded the IEEE MTT-S Outstanding Young Engineer Award; the ITG Award of German VDE, in 2017; and the IEEE Microwave Application Award, in 2025. He was the Chair of the IEEE MTT-S Technical Committee MTT-24, from 2018 to 2020. Since 2020, he has been the Vice Chair and elected member of the IEEE MTT-S/AP German Chapter Executive Board. He served as the Conference Chair for the 2020 German Microwave Conference, the Technical Program Chair for the IEEE Radio and Wireless Week 2021, and the General Chair for the IEEE Radio and Wireless Week 2023. He serves as a reviewer for several journals and conferences.